Uncertainty Analysis for the miniaturized laser heterodyne radiometer (mini-LHR)

G B Clarke,[1,2,*] E L Wilson,[2] J H Miller,[3] and H R Melroy,[2,3]

[1]American University, 4400 Massachusetts Avenue, Washington, DC, 20016, United States of America
[2]Laser Remote Sensing Laboratory, NASA Goddard Space Flight Center, 8800 Greenbelt Road, Greenbelt, Maryland, 20771, United States of America
[3]Department of Chemistry, George Washington University, 725 21ST Street, NW, Washington, DC, 20052, United States of America
*Corresponding author: gclarke@american.edu

Abstract. Presented here is a sensitivity analysis for the miniaturized laser heterodyne radiometer (mini-LHR). This passive, ground-based instrument measures carbon dioxide (CO_2) in the atmospheric column and has been under development at NASA/GSFC since 2009. The goal of this development is to produce a low-cost, easily-deployable instrument that can extend current ground measurement networks in order to (1) validate column satellite observations, (2) provide coverage in regions of limited satellite observations, (3) target regions of interest such as thawing permafrost, and (4) support the continuity of a long-term climate record. In this paper an uncertainty analysis of the instrument performance is presented and compared with results from three sets of field measurements. The signal-to-noise ratio (SNR) and corresponding uncertainty for a single scan are calculated to be 329.4±1.3 by deploying error propagation through the equation governing the SNR. Reported is an absorbance noise of 0.0024 for 6 averaged scans of field data, for an instrument precision of ~0.2 ppmv for CO_2.

1. Introduction

The miniaturized laser heterodyne radiometer (mini-LHR) [1-3] is a portable ground instrument that measures greenhouse gases in the atmospheric column that is under development at NASA Goddard Space Flight Center. While LHRs have been in common use at NASA for several decades [4, 5], development of the miniaturized version began in 2009 and regular measurements in the atmospheric column have been ongoing since 2012. In addition to testing at NASA, the instrument has been field tested at three sites to establish instrument performance: (1) the Total Column Carbon Observing Network (TCCON) site in Park Falls, Wisconsin (September 2012), (2) Castle Airport in Atwater, California (February 2013), and (3) the NOAA Mauna Loa Observatory in Hawaii (May 2013). Data comparisons with instruments at these sites will be the topics of future publications.

The mini-LHR operates in tandem with an AERONET [6] sun photometer - using its sun tracker as a platform for the mini-LHR light collection optics. AERONET is an established global network of more than 450 instruments [6-8] and provides a path for future mini-LHR deployments. This partnership offers a simultaneous measurement of aerosols, known to be important modulators in regional carbon cycles, and includes coverage in key artic regions.

In this paper, an estimation of absorbance noise for the mini-LHR is presented to validate the accuracy of the measurements by analyzing component level sources of error. The analysis resulted in a detailed characterization of

a signal-to-noise and uncertainty in measurement. The addition of the instrument noise, found through the SNR calculation, and the experimental error, found through the uncertainty of the measurement, yielded at total estimate for absorbance noise.

2. Description of the Mini-LHR Instrument Technique

The mini-LHR, shown in Figure 1, is a passive instrument that measures the concentration of CO_2 in the atmosphere through its absorption of sunlight in the infrared. Sunlight is collect using collimating optics (0.2º field of view) attached to the side of an AERONET sun tracker with a pointing stability of 0.1º, and then modulated with an optical chopper. The sunlight is then superimposed with light from a distributive feedback (DFB) laser (centered at 1611.51 nm) in a 50/50 single-mode fibre coupler, and then mixed in a fast (10 GHz) InGaAs photodiode. The resultant beat signal, or intermediate frequency signal, is amplified with a stage of RF (Radio Frequency) amplifiers and detected with a square-law detector that outputs a DC voltage proportional to the square of the input voltage. The RF output is further amplified and low-pass filtered through a video amplifier circuit. The final output is processed with a lock-in amplifier to measure the magnitude of the beat signal. As the laser is scanned across the CO_2 absorption feature, the magnitude of the beat signal is monitored [1].
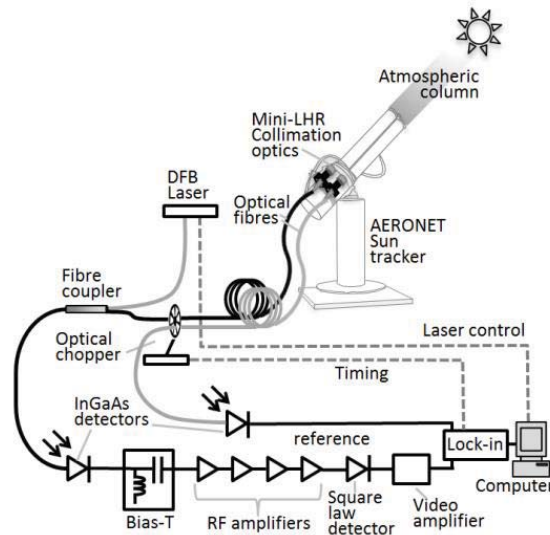

Figure 1 A schematic of the mini-LHR optical and electrical setup. Collimating Optics, attached to an AERONET suntracker, collect sunlight that has undergone absorption by CO_2. The sunlight is mixed with a DFB laser (local oscillator) in a fast InGaAs detector. The resultant beat signal is amplified by a series of amplifiers, and then detected by a square law detector. CO_2 absorption feature is measured by scanning the local oscillator across the feature and measuring the changes in amplitude of the beat signal.

The retrieval algorithm, developed at the George Washington University (GWU) [1, 9], converts the scanned absorption feature to a column mole fraction. In this algorithm, the atmosphere is modeled as a series of spherically symmetric shells with boundaries specified at defined altitudes. Profiles of atmospheric temperature, humidity, and pressure used in the retrieval algorithm are taken from the Modern-Era Retrospective Analysis for Research and Applications (MERRA)[10]. Spectra are then calculated for 100 m steps from ground level to 60 km. The resultant spectra are then fit using a Nelder-Mead simplex algorithm [11] iterating the CO_2 concentration, wavelength adjustment (to account for slight dither in laser calibration), and instrument bandwidth. A Multi-linear regression is then used to determine concentrations.

In the current instrument configuration column CO_2 is measured at ~1 minute intervals throughout the day during sunlight hours when clouds are not present. Figure 2 shows an example of a typical single data scan

collected in May 2013 at the NOAA Mauna Loa Observatory in Hawaii. The data is shown with a modeled fit of the absorption feature produced by the algorithm. The data was collect with an integration time of 500 ms for each data point. The scan stepped across the absorption feature at 0.01 nm increments for the wings, and 0.002 nm increments for the feature. The increased step magnitude on the wings was done to increase scan speed, to fit within AERONET observation window of ~1 minute.
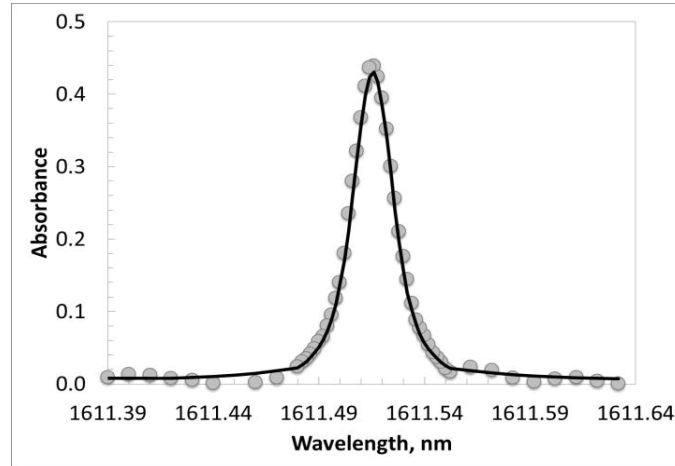

Figure 2 Shown is a typical scan of a CO_2 absorption feature that was collected at 10 a.m. on May 2013 at Mauna Loa Observatory, HI. Data points (dots) are shown with a fit from the retrieval algorithm (solid line).

3. Uncertainty Analysis

The following analysis calculates a value and uncertainty for the signal-to-noise ratio (SNR) for the mini-LHR in order to calculate the absorbance noise. The absorbance noise (Δ_{abs}) (fluctuations in the absorbance signal) is the combination of the instrument (systematic) noise (Δ_{sys}) and the experimental (random) noise (Δ_{ran}):

$$\Delta_{abs} = \Delta_{sys} + \Delta_{ran} \tag{1}$$

where $\Delta_{sys} = 1/SNR$ and $\Delta_{ran} = \Delta_{SNR}/SNR$ and Δ_{SNR} is the uncertainty in the SNR. The uncertainty in the SNR (Δ_{SNR}) was found by measuring uncertainties for each component in the instrument and tracking the propagation of the error. Sub-sections 3.1-3.5 provide detail for each of the component-level measurements.

For a laser heterodyning radiometer implementing a distributive feedback laser, the SNR is given as:

$$SNR = \frac{2\eta_e \sqrt{B\tau} \cdot T_0}{\exp\left(\dfrac{h\nu}{\kappa_B T_{BB}}\right) - 1} \tag{2}$$

where T_{BB} is the temperature of the black body, η_e is the effective quantum efficiency of the InGaAs photodiode, B is the bandwidth of the intermediate frequency (or IF), ν is the frequency, h is Planck's constant, κ_B is Boltzmann's constant, τ is the equivalent integration time and T_0 is the total transmission factor [12]. In this system the signal is proportional to the blackbody radiation (calculated via Planck's Law, and degraded by transmission loss and quantum efficiency of the detector), and the noise is proportional to the $1/\sqrt{B\tau}$ [13]. With values discussed below, and assuming a blackbody temperature of 5777 ± 10 K [14], a SNR of 329.4 is calculated, correlating to an instrument noise of 0.0030.

The uncertainty in the SNR, which is responsible for the random error for this instrument, is dependent on the component-level uncertainties. The error propagation is then calculated through:

$$\Delta q = \sqrt{(\; [dq/dx \; \Delta x]\,^2 + \cdots + \; [dq/dz \; \Delta z]\,^2)} \tag{3}$$

where Δq is the uncertainty of the SNR, dq/dx is the partial derivative of the SNR equation with respect to individual components of the equation, and Δx is the error that is associated with each component of the SNR equation [15]. The uncertainty in the SNR calculated through the error propagation is ± 1.3. This corresponds to a fractional uncertainty of the calculated signal, or random noise component of the instrument, of ~0.038.

3.1. IF Bandwidth (B)

The intermediate frequency (IF) bandwidth of the instrument is the range of beat frequencies that can be measured by the mini-LHR. The IF bandwidth was measured by beating two lasers together and measuring the beat signal. In this experiment the first laser was held at a constant wavelength (1611.51 nm) while the second laser was scanned across the range of 1611.38-1611.64 nm. The beat signal RMS (root mean squared) was plotted verses the intermediate frequency and fit with a Gaussian profile. This produced an instrument bandwidth of 1.4267 ± 0.0049 GHz.
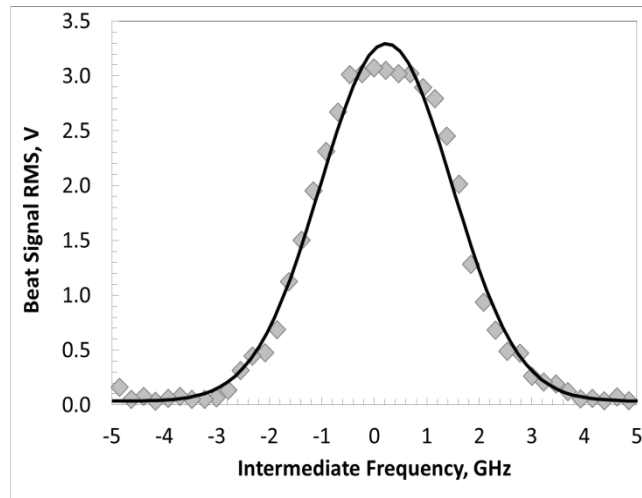

Figure 3 IF bandwidth measurement of the mini-LHR using two DFB lasers as described in section 3.3. Shown here the beat signal RMS (diamonds) is plotted as a function of the intermediate frequency, and fit with a Gaussian profile (solid line).

3.2. Integration Time (τ)

The uncertainty in the integration time was determined by analyzing an electric signal with a low duty cycle. A pulse generator was configured to send an electric pulse, at a relatively slow frequency (200 Hz) and a relatively small pulse width (5 μs), into the input of the lock-in amplifier. The lock-in amplifier could not "lock" onto the reference signal due to the small duty cycle (long time between pulses), and thus the "integration window" could be measured by digitizing the output of the lock-in amplifier. The resulting "integration window" was measured on an oscilloscope and was equal to twice the integration time (due to the lock-in amplifier sampling both positive and negative phases). Using an 80 μs integration time, a histogram of the "integration window" width was complied. The resulting error measurement from a Gaussian fit analysis produced associated uncertainty of 0.024%. For an integration time of 500 ms (consistent with the operation of the mini-LHR) there is an uncertainty in the measurement of 500±0.120 ms.

3.3. Total Transmission Factor (T_0)

The total transmission factor was determined by isolating the optical components of the mini-LHR, as shown in Figure 5. Light from a DFB laser, centered at 1611.51 nm (a) was first sent into a 50/50 fibre coupler/splitter (b). One end of the output was sent to a power meter (c) to monitor input power. The other end of the fibre coupler was sent into a collimator, to make it a compatible source for input into the optical components of the mini-LHR. Components (a)-(c) represent the input source, of known intensity, for the mini-LHR. Components (d)-(f) are the isolated optical components of the mini-LHR. The optical loss was determined by measuring the power at the exit point of this isolated system (g). Component (h) was a terminated fibre that was not in use. The optical loss was determined by the ratio of the power measured at (c) (input power) to the power measured at (g) (output power).
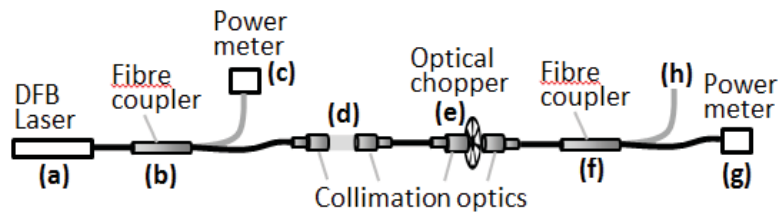

Figure 5 Optical setup for measuring transmission loss. An input source of known intensity (components a-c) was fed into the isolated mini-LHR optical setup (components d-f) to measure optical loss in the system at (g).

In addition optical fluctuations were measured in the input of the mini-LHR when in operation tandem to an AERONET sun photometer. The addition of this uncertainty yielded in a total transmission factor of 0.022±0.001

3.4. Frequency (ν)

The uncertainty in the frequency of the local oscillator of the mini-LHR was measured by recording the wavelength stability using an Optical Spectrum Analyzer (OSA). The central wavelength was set and measured for an extended period of time to simulate a full day of operation. This helps to include any long term changes in the laser operation into the uncertainty measurement. This measured value was converted to frequency with a final value of $(1.860322\pm.0000004)*10^{14}$ Hz.

3.5. Quantum Efficiency (η_e)

The photodiode sensitivity was measured by sending a 1611.51 nm laser into a 50/50 fibre splitter. One side of the splitter sent light to a power meter while the other side was directed into the photodiode. The photodiode was then connected to an oscilloscope to monitor the amplitude of the signal. Data was collected for an extended period of time to simulate a full day of data collection, and thus any drift or degradation would be incorporated into the error measurement. This value for photodiode sensitivity was then converted into quantum efficiency using the relationship of

$$R = \eta e / h\nu \tag{4}$$

where R is the measured responsivity, η is the quantum efficiency term that is in question, ν is the frequency, and h is Planck's constant [13]. This equation was rearranged such that it was solving for the quantum efficiency and then error was propagated through the equation using the general error propagation equation to arrive at a final uncertainty value for quantum efficiency of 0.5124±.0001.

4. Comparison of Analytical Analysis with Field Data

Using the previously discussed component errors (Section 3) and implementing them into the general error propagation equation, the SNR and error were calculated as 329.4 ± 1.3. This corresponds to an absorbance noise estimation of 0.0068, through the addition of instrument and experimental noise. These values are comparable to the current performance of the mini-LHR. Since its initial development in 2009, the mini-LHR has undergone significant changes to reducing error. The absorbance noise for a single random scan was seen to decrease from ~0.021 to ~0.009 to ~0.006 for field campaigns in Park Falls, Atwater, Mauna Loa respectively. Data sets from Mauna Loa show that the single scan performance is within 0.1% of calculated theoretical performance.

To correlate the noise in a typical scan to the detection limit in the column, a Monte-Carlo simulation was used to calculate the CO_2 concentration given varying levels of random noise. The concentration of CO_2 in the atmosphere was treated as a constant (at 390 ppmv) and the zenith angle was assumed to be 25°. The results of these simulations are shown in Figure 6 where the standard deviation in the calculated CO_2 concentration is plotted as a function of absorbance noise. An absorbance noise of 0.0068 corresponds to a sensitivity of ~0.6 ppmv assuming a 2 to 1 SNR.

It was possible to reduce error further by averaging consecutive. Figure 7 shows the number of averaged scans required to reach the lowest absorbance noise for each field test within a given hour. During the first field campaign at the Park Falls, the scan time was ~20 minutes and the lowest absorbance noise reached was 0.02 for an average of three scans (~1 hour of data). At the second field campaign in Atwater, the scan time was reduced to about 2 ½ minutes by transitioning from LabView to python software for data acquisition, resulting in a absorbance noise of about 0.003 by averaging about 45 minutes of data. During the third field campaign at Mauna Loa Observatory, the scan time was reduced to less than a minute and an absorbance noise of 0.0024 was reached in about 6 scans (~6 minutes of data). Once again referring to Figure 6 an estimated precision of ~0.2 ppmv is determined.
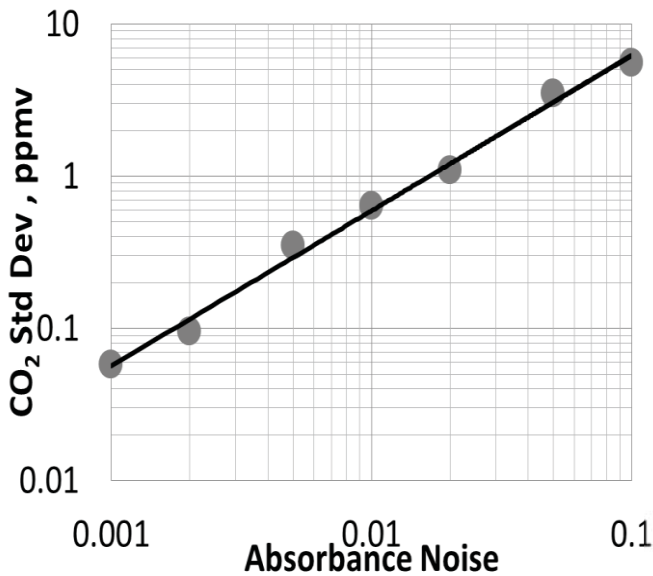

Figure 6 Noise in the absorbance signal is correlated to the sensitivity of the mini-LHR instrument. An absorbance noise of 0.0068 is equivalent to a column sensitivity of ~0.6 ppmv for ideal clear sky conditions.
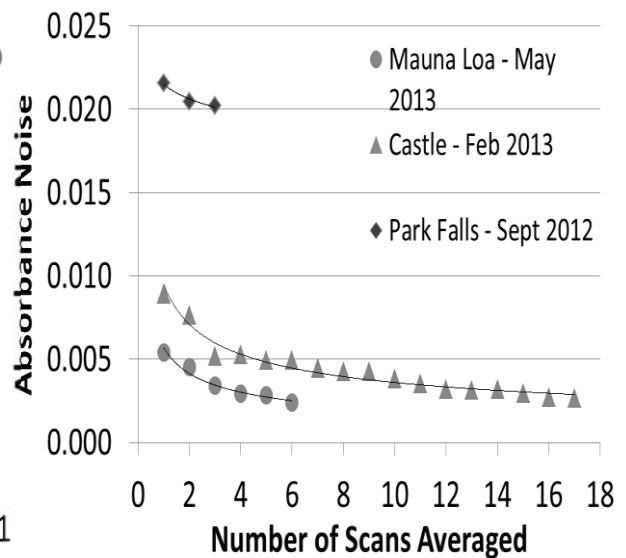
Figure 7 From September 2012 to May 2013, the mini-LHR absorbance noise has improved from 0.02 to 0.0024. Here, the absorbance noise is compared to the number of averaged scans.

5. Conclusions

In this paper a characterization and quantification of errors and uncertainties for the miniaturized laser heterodyne radiometer (mini-LHR) instrument has been presented through analytical analysis, yielding a signal-to-noise ratio of 329.4±1.3. The corresponding absorbance noise indicates a single scan performance of the mini-LHR that is within 0.1% of the calculated operational value. By averaging multiple scans, a column precision ~0.2 ppmv in molar column concentration of CO_2 was achieved.

6. References

[1]   Wilson EL, McLinden ML, Miller JH, Allen GR, Ott LE, Melroy HR, et al. Miniaturized Laser Heterodyne Radiometer for Measurements of CO2 in the Atmospheric Column. Applied Physics B: Lasers & Optics. Accepted March 2013.

[2]   Wilson EL, Clarke GB, Melroy HR, Miller JH, Allan GR, McLinden ML, et al., editors. A Miniaturized Laser Heterodyne Radiometer for a Global Ground-Based Column Carbon Monitoring Network. AGU Fall Meeting, Oral Presentation; 2012; San Francisco, CA: American Geophysical Union.

[3]   Wilson EL, McLinden ML, inventors MINIATURIZED LASER HETERODYNE RADIOMETER FOR CARBON DIOXIDE, METHANE AND CARBON MONOXIDE MEASUREMENTS IN THE ATMOSPHERIC COLUMN. USAFiled 2012.

[4]   Kostiuk T, Mumma MJ. Remote sensing by IR heterodyne spectroscopy. Applied Optics. 1983;22(17):2644-54.

[5]   Kostiuk T, Mumma MJ, Abbas MM, Buhl D. Sensitivity of an Astronomical Infrared Heterodyne Spectrometer. Infrared Physics. 1976;16:61-4.

[6]   AERONET Aerosol Robotic Network: NASA Goddard Space Flight Center; 2011. Available from: http://aeronet.gsfc.nasa.gov/.

[7]   Holben BN, Tanre D, Eck TF, Slutsker I, Abuhassan N, Newcomb WW, et al. An emerging ground-based aerosol climatology: Aerosol Optical Depth from AERONET. J Geophys Res. 2001;106:12 067-12 97.

[8]   Holben BN, Eck TF, Slutsker I, Tanre D, Buis JP, Setzer A, et al. AERONET - A federated instrument network and data archive for aerosol characterization. Remote Sensing of Environment. 1998;66:1-16.

[9]   Wilson EL, Georgieva EM, Heaps WS. Column Measurements of CO2, O2, and H2O by Differential Fabry-Perot Radiometer. American Geophysical Union, Fall Meeting. 2008.

[10]   Rienecker MM, et al. MERRA: NASA's Modern-Era Retrospective Analysis for Research and Applications. J Climate. 2011;24:3624-48.

[11]   Nelder JA, Mead R. A simplex method for function minimization. The Computer Journal. 1965;7:308-13.

[12]   Ku RT, Spears DL. High-sensitivity infrared heterodyne radiometer using a tunable-diode-laser local oscillator. Optics Letters. 1977;1(3):84-6.

[13]   Hobbs PCD. Building Electro-Optical Systems. Hoboken, New Jersey: John Wiley and Sons, Inc; 2009.

[14]   Ramírez I, Meléndez J. The Effective Temperature Scale of FGK STARS. II. T_{eff}: [Fe/H] Calibrations. The Astrophysical Journal. 2005;626(1):465-85.

[15]   Taylor JR. An Introduction to Error Analysis: The Study of Uncertainties in Physical Measurements. Second ed. Sausalito, California: University Science Books; 1997.